Ab Initio Chemical Kinetics for Reactions of H Atoms with SiH_x (x = 1–3) Radicals and Related Unimolecular Decomposition Processes

Putikam Raghunath,[a] Yun-Min Lee,[b] Shang-Ying Wu,[b] Jong-Shinn Wu,[b] and Ming-Chang Lin*[a]

Hydrogen atoms and SiH_x (x = 1–3) radicals coexist during the chemical vapor deposition (CVD) of hydrogenated amorphous silicon (a-Si:H) thin films for Si-solar cell fabrication, a technology necessitated recently by the need for energy and material conservation. The kinetics and mechanisms for H-atom reactions with SiH_x radicals and the thermal decomposition of their intermediates have been investigated by using a high high-level *ab initio* molecular-orbital CCSD (Coupled Cluster with Single and Double)(T)/CBS (complete basis set extrapolation) method. These reactions occurring primarily by association producing excited intermediates, $^1SiH_2$, $^3SiH_2$, SiH_3, and SiH_4, with no intrinsic barriers were computed to have 75.6, 55.0, 68.5, and 90.2 kcal/mol association energies for x = 1–3, respectively, based on the computed heats of formation of these radicals. The excited intermediates can further fragment by H_2 elimination with 62.5, 44.3, 47.5, and 56.7 kcal/mol barriers giving ^1Si, ^3Si, SiH, and $^1SiH_2$ from the above respective intermediates. The predicted heats of reaction and enthalpies of formation of the radicals at 0 K, including the latter evaluated by the isodesmic reactions, $SiH_x + CH_4 = SiH_4 + CH_x$, are in good agreement with available experimental data within reported errors. Furthermore, the rate constants for the forward and unimolecular reactions have been predicted with tunneling corrections using transition state theory (for direct abstraction) and variational Rice–Ramsperger–Kassel–Marcus theory (for association/decomposition) by solving the master equation covering the P,T-conditions commonly employed used in industrial CVD processes. The predicted results compare well experimental and/or computational data available in the literature. © 2013 Wiley Periodicals, Inc.

DOI: 10.1002/qua.24396

Introduction

Chemical vapor deposition (CVD) is one of the most extensively performed processes for thin-film growth of hydrogenated amorphous silicon (a-Si:H),[1] polycrystalline silicon (p-Si),[2] and silicon nitride (SiN_x).[3] These materials have been widely applied in devices such as solar cells, thin-film transistors for liquid crystals, and light emitting diodes, and protection films of semiconductor devices.[4,5] In the Si-solar cell manufacturing industry, the employment of a-Si:H thin films for cell fabrication has recently gained considerable interest due to the need for energy and material conservation. The a-Si:H thin films can be manufactured by CVD at a lower cost with hydrogen passivation that effectively reduces the dangling bond density by several orders of magnitude affording a sufficiently low amount of defects for device fabrications.

CVD processes such as plasma-enhanced CVD (PECVD) or catalytically enhanced CVD (Cat-CVD) for deposition of a-Si:H films are very complicated; they involve intertwining gas-phase and surface reactions. Characteristics of deposited films are largely affected by the plasma density (in PECVD) or the hot wire configuration and temperature (in Cat-CVD), as well as the fluxes and varieties of the precursor molecules transported by gas flow, following electrical discharge or catalytic decomposition over a hot wire, onto substrates. In the case of the PECVD of a-Si:H using SiH_4 and H_2 as precursor gases, H atoms and SiH_x (x = 1–3) radicals may coexist in high concentrations by collisions between energetic electrons and molecules; the reactions between these reactive species may play a pivotal role in film growth at the substrate. To further refine the technology to ensure uniform growth of an a-Si:H film over a large substrate area, chamber-scale modeling is inevitable; it can help delineate and control the intricate coupling plasma and thermal field with the complex Si-chemistry. Therefore, it is important to understand the reactions involved quantitatively for successful development and better applications of the technology.

The kinetics and mechanisms for the reactions of H atoms with the SiH_x radicals present in the SiH_4 PECVD process remain largely unknown; these radicals have been experimentally detected under various conditions,[6–11] and qualitatively the life time of SiH_3 was found to be much longer than those of SiH and SiH_2 in plasma media.[12,13] The mechanism and rate constant for SiH_4 decomposition reaction have been studied theoretically by various groups.[14–23] Chemical properties and some kinetic information regarding SiH (silylidyne), SiH_2 (silylene), and SiH_3 (silyl) have been discussed previously by

[a] *P. Raghunath, M. C. Lin*
Center for Interdisciplinary Molecular Science, Department of Applied Chemistry, National Chiao Tung University, Hsinchu 300, Taiwan
[b] *Y. M. Lee, S. Y. Wu, J. S. Wu*
Department of Mechanical Engineering, National Chiao Tung University, Hsinchu 300, Taiwan
E-mail: chemmcl@emory.edu

Contract grant sponsor: Taiwan's National Science Council (NSC); Contract grant number: NSC100-2113-M-009-013 (to M.C.L. and P.R.).
Contract grant sponsor: Ministry of Economics; Contract grant number: 98-EC-17-A-07-S2-0043 (to S.Y.W. and J.S.W.).

Jasinski et al.[24] They also summarized several experimental methods for the detection and monitoring of these radicals and provided the enthalpies of formation of these radicals. Gordon et al.[25] have applied *ab initio* quantum mechanical methods to study the SiH insertion into the H_2 molecule. Walch and Dateo[21] have studied various reactions relevant to the thermal decomposition of SiH_4, SiH_3, $SiClH_3$, $SiCl_2H_2$, and $SiCl_3H$. Recently, we have theoretically interpreted the decomposition of silane up to Si_3H_8 by the reactions with hydrogen atoms and SiH_3 giving various products and also calculated their heats of formation of larger silalyl radicals for comparison with available experimental data.[26]

The generated radicals and ions in a PECVD chamber may undergo various kinds of reactions with silane, before they reach the substrate. For H and SiH_x ($x = 1$–3) radical species, they may interact with one another by the following chemical reactions in the forward and reverse directions:

$$H + SiH_3 \rightarrow SiH_4{}^* \rightarrow SiH_4 \quad (1a)$$

$$\rightarrow SiH_2 + H_2 \quad (1b)$$

$$H + SiH_2 \rightarrow SiH_3{}^* \rightarrow SiH_3 \quad (2a)$$

$$\rightarrow SiH + H_2 \quad (2b)$$

$$H + SiH \rightarrow SiH_2{}^* \rightarrow SiH_2 \quad (3a)$$

$$\rightarrow {}^3Si + H_2 \quad (3b)$$

$$\rightarrow {}^1Si + H_2 \quad (3c)$$

In the above reaction schemes, "*" denotes an internally activated intermediate that can fragment into smaller radicals by dehydrogenation or be collisionally deactivated to give SiH_x. The kinetics of these reactions, albeit simple mechanistically, have not been experimentally or computationally studied systematically; for example, what are the effects of temperature and pressure on the competing processes that are critical to a faithful and realistic simulation of a-Si:H thin-film growth by PECVD or Cat-CVD process.

In this work, the potential energy surfaces (PESs) of the title reactions have been predicted by high-level *ab initio* molecular-orbital (MO) calculations. Furthermore, the enthalpies of formation of the SiH_x species have been reliably predicted and compared with available experimental data to validate our calculated heats of reaction. The temperature and pressure dependences of the rate constants for the forward and its related unimolecular processes have been derived using variational Rice–Ramsperger–Kassel–Marcus (RRKM) theory by solving the master equation covering the conditions commonly used in industrial deposition of a-Si:H films.

Computational Methods

Ab Initio MO calculations

The various stationary points (minima or saddle points) on the PES for H-atom reactions with the three SiH_x radicals were optimized using CCSD(T)/6-311+G(d,p) basis set and for improved energies, single-point calculations at the CCSD(T)/6-311++G(3df,3pd) level of theory[27] were used. The vibrational frequencies were determined at the same levels of theories to obtain zero-point energy (ZPE) corrections and to characterize the stationary points. Based on the CCSD(T) optimized geometries, the PES was calculated and mapped using the CCSD(T)/CBS method,[28] in which the basis set extrapolation was based on the calculations with the aug-cc-pVXZ (X = D, T, and Q) basis sets of Dunning.[29] The Gaussian 03 quantum chemical software was used in each of these evaluations.[30] The CBS energies have been estimated using three-point extrapolation scheme,

$$E(X) = E_{CBS} + b\ \exp[-(X-1)] + c\ \exp[-(X-1)^2] \quad (1)$$

where X is the cardinal number of the basis sets associated with $X = 2$ (DZ) (double Zeta), 3 (TZ) (triple Zeta) 4 (QZ) (quadruple Zeta) and E_{CBS} is the asymptotic value, which is taken to approximate the CBS limit.

Rate constant calculations

The rate constants were calculated using the microcanonical transition-state theory (TST) and the RRKM theory by solving the one-dimensional master equation to derive the nonequilibrium distribution function for each channel with the VARIFLEX program suite.[31] For a barrierless association/decomposition process, the variational TST (VTST)[32] was approximated with the Morse function, $V(R) = D_e\ \{1 - \exp[-\beta\ (R - R_e)]\}^2$, in conjunction with a potential anisotropy function to represent the minimum potential energy path (MEP), which will be discussed later. Here, D_e is the binding energy excluding zero-point vibrational energy for an association reaction, R is the reaction coordinate (i.e., the distance between the two bonding atoms), and R_e is the equilibrium value of R at the stable intermediate structure. For a loose transition-state process, the potential for the transitional degrees of freedom orthogonal to the reaction coordinate is described in terms of internal angle with sinusoidal functions.[33] The coefficient in the potential expression can be determined by the appropriate force constant matrix [$F_{ij}(R)$] at the potential minimum, assuming that $F_{ij}(R)$ decays exponentially with the bond distance:

$$F_{ij}(R) = F_{ij}(R_0)\exp[-\eta(R - R_0)]$$

Here, R is the bond distance along with the reaction coordinate; R_0 is the bond distance at the equilibrium structure; and η is a decay parameter with R increasing. For a spin forbidden crossing reaction, we apply the nonadiabatic TST[34,35] to estimate its crossing probability. The procedure is given in the Supporting Information.

Results and Discussion

PESs and reaction mechanisms

Figure 1 presents the PESs of the three SiH_x reactions with H atoms based on the energies obtained with the CCSD(T)/6-311+G(d,p)/CBS method. The optimized geometric parameters of reactants, intermediates, and transition states computed at

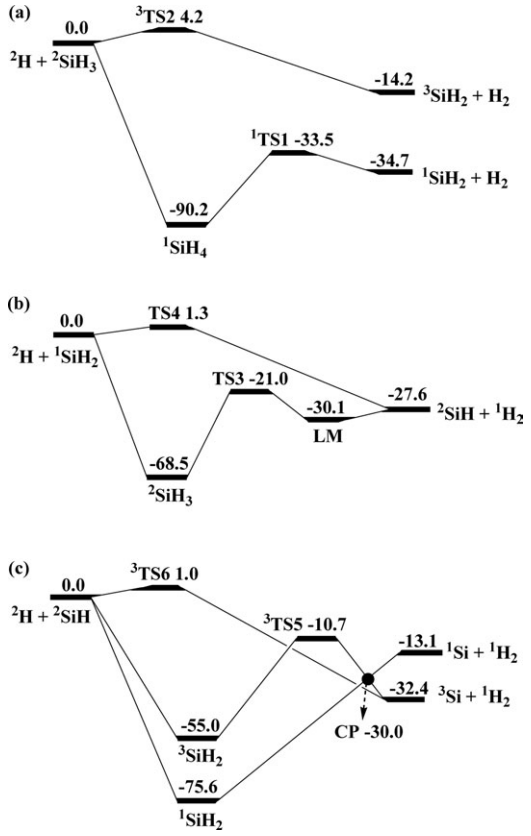

Figure 1. Potential energy profiles of H reactions with SiH_x (x = 1–3) in units of kcal/mol. Relative energies with ZPVE are calculated at the CCSD(T)/6-311+G(d,p)/CBS level.

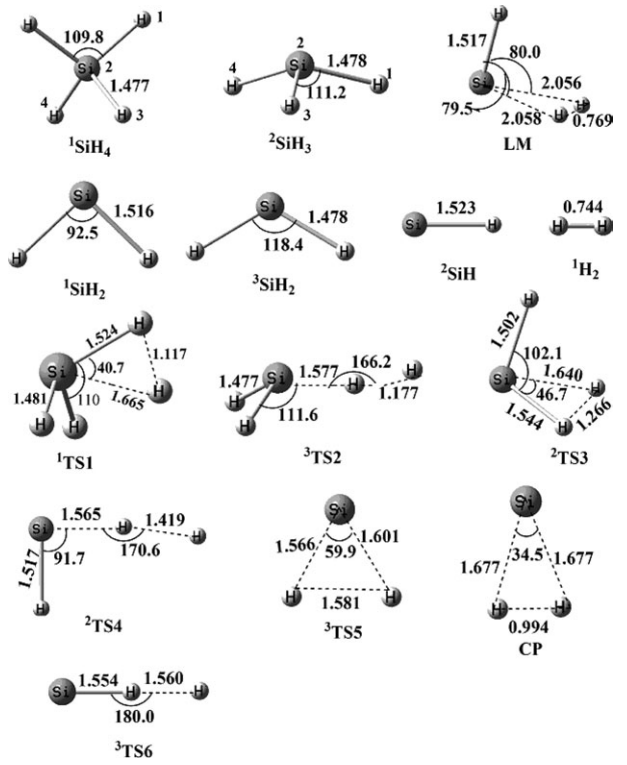

Figure 2. The optimized geometries of the reactants, transition states, and products calculated at the CCSD(T)/6-311+G(d,p) level.

the CCSD(T)/6-311+G(d,p) level and their structures are presented in Figure 2. The corresponding energies estimated at different levels of the theory are summarized in Table 1. The rotational constants and vibrational frequencies of the various stationary points predicted at the CCSD(T)/6-311+G(d,p) level are given in Table 2. The calculated heats of reaction and formation values compared with experimental data at 0 K are given in Table 2. The following discussion will be based on the results computed at the CCSD(T)/CBS level, and all the energies of TSs and intermediates are relative to the reactants. In Table 2, the values of T1 diagnostics for all the structures are calculated at the CCSD(T)/6-311+G(d,p) level, and the results are within 0.006–0.025 range, suggesting that our single-reference results are reasonable.

H + SiH_3 reaction. The initial association mechanism of the H atom with SiH_3 leading to SiH_4 as shown in Figure 1a was predicted to be exothermic by 90.2 kcal/mol, which is close to the experimental Si—H bond energy 88.9 ± 1.2 kcal/mol as listed in Table 3. For SiH_4, its Si—H bond length, 1.477 Å, is also in close agreement with the experimental value, 1.481 Å. This association process does not have a well-defined transition state; its associated potential function was computed variationally to cover the range of Si—H bond separations in the forming SiH_4 from 1.477 to 5.677 Å with the second-order multireference perturbation theory (CASPT2) based on the CASSCF (Complete Active Space Self-Consistent Field) optimized geometries with eight active electrons and eight active orbitals using the 6-311+G(3df,2p) basis set. Other geometric parameters were fully optimized. These calculations were performed with the MOLPRO code.[36] The calculated potential energy curve can be fitted to the Morse function with the parameter of β = 1.872 $Å^{-1}$, and the estimated decay parameters of internal angles corresponding to the vicinity of variational

Table 1. Calculated relative energies (kcal/mol, ZPE corrections are included) for the H atom reactions with SiH_x (x = 1–3) at various levels of theory.

Reactions	CCSD(T)/ 6–311+G(d,p)	CCSD(T)/ 6–311++G(3df,3pd)// CCSD(T)/6–311+G(d,p)	CCSD(T)/ CBS
$^2H + {}^2SiH_3$	**0.0**	**0.0**	**0.0**
$^1SiH_4$	−86.8	−89.0	−90.2
TS1	−27.8	−32.1	−33.5
$^1SiH_2 + {}^1H_2$	−33.2	−34.9	−34.7
^{3}TS2	5.7	4.4	4.2
$^3SiH_2 + {}^1H_2$	−14.8	−14.7	−14.2
$^2H + {}^1SiH_2$	**0.0**	**0.0**	**0.0**
$^2SiH_3$	−66.4	−67.3	−68.5
TS3	−16.6	−19.8	−21.0
^{2}LM	−27.6	−29.7	−30.1
$^2SiH + {}^1H_2$	−28.0	−28.1	−27.6
TS4	2.5	1.5	1.3
$^2H + {}^2SiH$	**0.0**	**0.0**	**0.0**
$^1SiH_2$	−71.5	−74.1	−75.6
$^3SiH_2$	−53.1	−53.9	−55.0
$^1Si + {}^1H_2$	−9.0	−12.5	−13.1
$^3Si + {}^1H_2$	−33.8	−33.1	−32.4
^{3}TS5	−6.9	−10.9	−10.7
^{3}TS6	1.9	1.1	1.0
CP	−25.3	−29.1	−30.0

Table 2. Calculated vibrational frequencies of the species involved in the H atom reactions with SiH_x (x = 1–3) computed at CCSD(T)/6–311+G(d,p) level.

Species	Frequencies (cm^{-1})	Rotational constants (cm^{-1})	T1 diag.	Symm. No.
$^1SiH_4$	955, 955, 955, 991, 991, 2292, 2297, 2297, 2297	2.872, 2.872, 2.872	0.009	12
$^2SiH_3$	799, 956, 956, 2263, 2297, 2297	4.752, 4.752, 2.811	0.010	3
^{2}LM	126, 280, 743, 881, 2087, 3992	6.841, 2.106, 1.707	0.019	1
$^1SiH_2$	1042, 2095, 2099	8.149, 6.964, 3.755	0.014	2
$^3SiH_2$	900, 2236, 2297	15.628, 5.186, 3.894	0.013	2
^{2}SiH	2063	7.468	0.015	1
$^1H_2$	4421	60.475	0.006	2
^{1}TS1	*i*1225, 751, 767, 987, 1050,1606, 2164, 2258, 2280	3.439, 2.692, 2.309	0.014	1
^{3}TS2	*i*1305, 288, 421, 781, 936, 990, 1261, 2265, 2300	4.650, 1.532, 1.242	0.016	1
^{2}TS3	*i*1371, 717, 968, 1611, 1953, 2150	5.626, 3.705, 2.584	0.043	1
^{2}TS4	*i*792, 134, 283, 1006, 1469, 2098	7.474, 1.576, 1.302	0.020	1
^{3}TS5	*i*644, 1630, 1876	13.389, 4.757, 3.51	0.025	2
^{3}TS6	*i*572, 210, 398, 1620	1.468	0.019	1
CP	*i*221, 1649, 1774	33.80, 3.49,3.16	0.016	2

transition state are η(H3Si2H1) = 1.029 $Å^{-1}$ and η(H4H3Si2H1) = 1.005 $Å^{-1}$, which will be used later for rate constant calculations. The excited SiH_4 product can decompose to form SiH_2 + H_2 with 56.7 kcal/mol barrier via TS1. Previous results show that the barrier energy is 6.7 kcal/mol lower using a semiempirial method,[15] and other two calculations are in good agreement with the 59.9 kcal/mol barrier predicted with CCSD(T)/aug-cc-pvtz basis set extrapolation to the basis set limit at the MP2 level[21] and 57.0 kcal/mol barrier calculated at the CCSD(T)/CBS level.[23] The endothermicity of this process is 55.5 kcal/mol, and the overall enthalpy change for H + SiH_3 → SiH_2 + H_2 is predicted to be −34.7 kcal/mol, which is in close agreement with the experimental value, −33.9 ± 1.2 kcal mol. The calculation shows that the direct hydrogen abstraction reaction occurs by the attack of the H atom at one of the Si—H bonds of SiH_3 to produce $^3SiH_2$ + H_2 via triplet transition state TS2 with a 4.3 kcal/mol barrier energy. It is worth noting that we have also performed an extensive search for a roaming transition state of the H + SiH_3 reaction directly leading to the formation of $^1SiH_2$ + H_2, but our attempts failed to locate the existence of such a loose RTS (Roaming transition state), which may compete with the very fast association/decomposition process via SiH_4 and TS1.

H + SiH_2 reaction. A schematic potential energy diagram for the H + $^1SiH_2$ reaction is shown in Figure 1b; the reaction can occur in two possible pathways. The first mechanism occurred through association of H and $^1SiH_2$ to form SiH_3 barrierlessly with 67.3 and 68.5 kcal/mol exothermicities predicted at the CCSD(T)/6-311++G(3df,3pd)//CCSD(T)/6-311+G(d,p) and CCSD(T)/CBS levels, respectively. The latter agrees better with the experimental value of 69.5 ± 1.2 (see Table 3). We optimized SiH_3 geometry with C_{3v} symmetry. The SiH_3 radical can further dissociate with 47.5 kcal/mol barrier energy (TS3), which lies 9.1 and 6.6 kcal/mol above the product complex (LM, SiH…H_2) and SiH + H_2 products, respectively. The transition state barrier for SiH + H_2 → SiH_3, 6.6 kcal/mol, is in good agreement with the estimation of Gordon et al.,[25] 5.6 ± 1 kcal/mol (with ZPE correction). Walch and Dateo[21] also have studied the same reaction and estimated a barrier height of 6 kcal/mol at the CCSD(T)/a-cc-pVTZ level of theory with extrapolation to the complete basis set (CBS) limit by the MP2 method. The second reaction is direct hydrogen abstraction from one of hydrogen atoms of $^1SiH_2$ to produce ^{2}SiH + H_2 through TS1 with 1.3 kcal/mol barrier. The formation of SiH_3 from H + $^1SiH_2$ is a barrierless association process, as shown in Figure 1b. Its associated potential function was computed variationally to cover the range of Si—H separation from 1.5 to 5.5 Å at the CASPT2(7,9)/6-311+G(3df)//CASSCF(7,9)/6-311+G(3df) level. The computed potential energies could be fitted to the Morse function with the parameter β = 2.902 $Å^{-1}$. Estimated decay parameters of internal angles corresponding to vicinity of variational transition state are η(H3Si2H1) = 1.089 $Å^{-1}$ and η(H4H3Si2H1) = 0.73 $Å^{-1}$.

H + SiH reaction. The PES of the H + SiH system shown in Figure 1c has been computed at the CCSD(T)/CBS level also. On the PES, there are two possible mechanisms for H atom reactions with the SiH radical; one occurs by direct abstraction, involving a colinear SiHH structure, and the other occurs barrierlessly forming the excited SiH_2 radical followed by dehydrogenation to give Si + H_2. The barrier to the linear H-abstraction TS6 via the triplet path is predicted to be 1.0 kcal/mol relative to SiH + H, or 33.3 kcal/mol relative to ^{3}Si + H_2. The association reactions producing singlet and triplet states of SiH_2 take place without intrinsic barriers and are predicted to be exothermic by 75.6 and 55.0 kcal/mol, respectively, which agree excellently with experimental heats of reaction 75.7 ± 0.5 and 54.7 ± 0.5 kcal/mol at 0 K (see Table 3). For barrierless association reactions of H with SiH producing the singlet SiH_2, we computed variationally the Si—H separation from 1.5 to 5.5 Å at an interval of 0.1 Å using the CASPT2(6,7)/6-311+G(3df)//CASSCF(6,7)/6-311+G(3df) method; the predicted MEP was fitted to the Morse function with β = 1.76 and 3.38 $Å^{-1}$. The Morse potential for the dissociation reaction $^1SiH_2$ → ^{1}Si + H_2 was determined to be β = 4.44 $Å^{-1}$.

The predicted energy difference between singlet and triplet splitting energy of SiH_2 at the CCSD(T)/CBS level is 20.6 kcal/mol, which is also in close agreement with the experimental value, 21.0 ± 0.7 kcal/mol.[37a] The ^{1}Si + H_2 products may be produced by the direct dissociation of the $^1SiH_2$ radical with predicted dissociation energy 62.5 kcal/mol without an intrinsic

Table 3. Heats of reaction ($\Delta_r H_0^\circ$) and heats of formation ($\Delta_f H_0^\circ$) of species at 0 K predicted at the CCSD(T)/6–311+G(d,p)/CBS level of theory given in kcal/mol.

		Heat of reaction $\Delta_r H_0^\circ$		Heat of formation $\Delta_f H_0^\circ$	
Species	Reactions[a]	Calculated	Experimental	Calculated	Experimental
$^2SiH_3$	$^1SiH_4 \rightarrow {}^2H + {}^2SiH_3$	90.2	88.9 ± 1.2	49.0	47.7 ± 1.2
$^1SiH_2$	$^1SiH_4 \rightarrow {}^1SiH_2 + {}^1H_2$	55.5	55	66.0	65.6 ± 0.7
$^1SiH_2$	$^2H + {}^2SiH_3 \rightarrow {}^1SiH_2 + {}^1H_2$	−34.7	−33.9 ± 1.2	64.7 ± 1.2	65.6 ± 0.7
$^2SiH_3$	$^2SiH_3 \rightarrow {}^2H + {}^1SiH_2$	68.5	69.5 ± 1.2	48.8 ± 0.7	47.7 ± 1.2
^2SiH	$^2SiH_3 \rightarrow {}^2SiH + {}^1H_2$	40.9	41.9 ± 1.2	88.6 ± 1.2	89.6 ± 1.2
$^1SiH_2$	$^2H + {}^1SiH_2 \rightarrow {}^2SiH + {}^1H_2$	−27.6	−27.6	65.5 ± 1.2	65.6 ± 0.7
$^1SiH_2$	$^1SiH_2 \rightarrow {}^2H + {}^2SiH$	75.6	75.7	65.7 ± 1.2	65.6 ± 0.7
$^3SiH_2$	$^3SiH_2 \rightarrow {}^2H + {}^2SiH$	55.0	54.7	86.3 ± 1.2	86.6 ± 0.7
^3Si	$^3SiH_2 \rightarrow {}^3Si + {}^1H_2$	22.6	20 ± 1.2	109.2 ± 0.7	106.6 ± 1.9
^1Si	$^1SiH_2 \rightarrow {}^1Si + {}^1H_2$	62.5	–	128.1 ± 0.7	124.6 ± 1.9
^3Si	$^2H + {}^2SiH \rightarrow {}^3Si + {}^1H_2$	−32.4	−34.8	108.9 ± 1.2	106.6 ± 1.9
^1Si	$^2H + {}^2SiH \rightarrow {}^1Si + {}^1H_2$	−13.1	–	128.2 ± 1.2	124.6 ± 1.9
^2SiH	$^2SiH + {}^1CH_4 \rightarrow {}^1SiH_4 + {}^2CH$	76.8	78.1	90.2	89.6 ± 1.2
$^1SiH_2$	$^1SiH_2 + {}^1CH_4 \rightarrow {}^1SiH_4 + {}^1CH_2$	62.0	63.4	66.9	65.6 ± 0.7
$^3SiH_2$	$^3SiH_2 + {}^1CH_4 \rightarrow {}^1SiH_4 + {}^3CH_2$	32.6	–	86.2	86.6 ± 0.7
$^2SiH_3$	$^2SiH_3 + {}^1CH_4 \rightarrow {}^1SiH_4 + {}^2CH_3$	12.5	14.4	49.6	47.7 ± 1.2 49.0[b]

[a] The experimental values used in the calculations are obtained based on the enthalpies of formation at 0 K for H = 51.7 kcal/mol; H_2 = 0.0 kcal/mol ; SiH_4 = 10.5 kcal/mol[39]; SiH_3 = 47.7 ± 1.2 kcal/mol[40]; $^1SiH_2$ = 65.6 ± 0.7 kcal/mol[37a]; SiH_2 and Si singlet–triplet splitting energy is 21.0 ± 0.7 and 18.01 kcal/mol,[37] respectively; SiH = 89.6 ± 1.2 kcal/mol[37a]; ^3Si = 106.6 ± 1.9 kcal/mol[39]; CH = 141.2 kcal/mol[39]; $CH_2(^3B_1)$ = 92.3 kcal/mol[39]; $CH_2(^1A_1)$ = 102.4 kcal/mol[41]; CH_3 = 35.6 kcal/mol[39]; (CH_4 = −16.0 kcal/mol.[39] [b] Ref. [26a] (calculated at the CCSD(T)/6–311++G(3df,2p)//CCSD(T)/6–311+G(d,p) level).

barrier. The singlet ^1Si atom may be deactivated to its ground triplet state ^3Si by collisional quenching during the reaction. As shown in the PES, the dissociation of the $^3SiH_2$ intermediate to $^3Si + H_2$ can occur by overcoming a 44.3 kcal/mol barrier at TS5 with 32.7 kcal/mol exothermicity. Our predicted barrier energy is in good agreement with a previous theoretical value 44.7 kcal/mol computed by PMP4/6-31++G(3d,3p)//HF/6-31G* + ZPVE.[38] Furthermore, the exothermicity of the product channel $^3Si + H_2$, 32.4 kcal/mol, is close to the experimental value, 34.8 kcal/mol. The energy difference between singlet and triplet states of Si atom at the CCSD(T)/CBS level is 19.3 kcal/mol, which is also in reasonable agreement with the experimental value, 18.01 kcal/mol.[37b] As shown in Figure 1c, there exists a crossing point (CP) between the triplet and singlet SiH_2 dissociation curves. To search for the CP, the minimum energy path for $^1SiH_2 \rightarrow {}^1Si + H_2$ was calculated along the reaction coordinate of ∠H—Si—H angle reduced from 92.5 to 14° with a step size of 2.0° at the CCSD(t)/6-311+G(d,p) level. Similarly, for triplet SiH_2 case, minimum energy path was calculated along the reaction coordinate of ∠H—Si—H angle decreases from 118.4 to 14° with a step size of 2.0° separated to $^3Si + H_2$. The reaction coordinate for the CP was obtained at ∠H—Si—H = 32.9°. The CP geometry was reoptimized at the CASSCF(6,6,Slaterdet)/ 6-311+G(3df,2p) level. Finally, the single-point energy for the CP with a 45.6 kcal/mol barrier from $^1SiH_2$ was obtained at the CCSD(T)/CBS level based on the optimized geometry using the CASSCF method.

Enthalpies of the formation

To validate the energetics for reliable prediction of rate constants, the predicted values of heats of formation ($\Delta_f H^\circ$) of all the species related to $H + SiH_x$ reactions have been calculated based on enthalpies of reaction at the CCSD(T)/6-311+G(d,p)/CBS level with experimental values of $\Delta_f H^\circ$ (0 K) from the NIST-JANAF tables[39] and the relevant literature.[24,40,41] Furthermore, isodesmic (bond and spin conserving) reactions, such as $^2SiH + {}^1CH_4 \rightarrow {}^1SiH_4 + {}^2CH$, $^{1,3}SiH_2 + {}^1CH_4 \rightarrow {}^1SiH_4 + {}^{1,3}CH_2$, and $^2SiH_3 + {}^1CH_4 \rightarrow {}^1SiH_4 + {}^2CH_3$ allowing the cancellation of computed errors are also used to confirm the calculated heats of formation at 0 K. The predicted heats of formation of all the species are presented in Table 3. The two sets of $\Delta_f H^\circ$ (0 K) values presented in Table 3 for ^2SiH, 88.6 ± 1.2 and 90.2 kcal/mol, $^1SiH_2$, 66.0 and 66.9 kcal/mol, SiH_3, 49.0 and 49.6 kcal/mol, were obtained by the corresponding unimolecular dissociation processes and isodesmic reactions, respectively. The results obtained by the CBS method agree closely with existing experimental data listed in the Table 3. The 20.6 kcal/mol triplet–singlet energy difference of SiH_2 also agrees well with the experimental value, 21.0 ± 0.7 kcal/mol.[37a] It is interesting to note that comparing with the analogous CH_2 radical, not only the spins of the two lowest electronic states are reversed but also the energy difference appears to be very large (8.8 kcal/mol for the singlet–triplet splitting in CH_2 versus 20.6 kcal/mol for the triplet–singlet splitting in SiH_2).

Rate Constant Calculations

The rate constants for the bimolecular reactions of H and SiH_x radicals and related unimolecular decomposition processes can be computed with the predicted PES using energies obtained by CCSD(T)/CBS extrapolation. For the H—SiH_x bond breaking process without an intrinsic barrier, we apply the VTST method

Table 4. Arrhenius parameters[a] for bimolecular reaction of H with SiH_x (x = 1–3) at various pressures including high-pressure limit (k_∞) and low-pressure limit (k_0).

	P (Torr)	A	n	E_a/R (K)	k_P (500 K)
$SiH_3 + H \rightarrow SiH_4$ (k_{1a})	k_∞	3.32×10^{-10}	−0.03	74	2.3×10^{-10}
	k_0	8.90×10^{-19}	−5.32	1676	1.21×10^{-34}
	0.3	2.44	−6.31	1672	6.99×10^{-19}
	1	8.43	−6.32	1675	2.33×10^{-18}
	10	8.82×10^{1}	−6.32	1677	2.36×10^{-17}
	760	8.87×10^{3}	−6.34	1628	2.26×10^{-15}
$SiH_3 + H \rightarrow SiH_2 + H_2$ (k_{1b})	10^{-3}–$10^{4}b$	3.55×10^{-10}	−0.05	77	2.3×10^{-10}
	10^{-3}–$10^{4}c$	1.86×10^{-8}	−0.54	593	
$SiH_3 + H \rightarrow {}^3SiH_2 + H_2$ (k_{TS2})		9.43×10^{-18}	2.28	765	2.83×10^{-12}
${}^1SiH_2 + H_2 \rightarrow SiH_4$	k_∞	1.66×10^{-17}	1.65	−832	2.73×10^{-12}
	k_0	7.04×10^{-18}	−4.44	1202	6.16×10^{-31}
	0.3	2.07×10^{1}	−5.44	1208	3.55×10^{-15}
	1	7.25×10^{1}	−5.44	1223	1.16×10^{-14}
$SiH_2 + H \rightarrow SiH_3$ (k_{2a})	k_∞	3.24×10^{-11}	0.47	84	5.05×10^{-10}
	k_0	7.62×10^{-24}	−3.51	1158	2.32×10^{-34}
	0.3	3.05×10^{-5}	−4.54	1135	1.64×10^{-18}
	1	1.11×10^{-4}	−4.54	1132	5.76×10^{-18}
	10	1.38×10^{-3}	−4.56	1131	6.44×10^{-17}
	760	1.91×10^{-1}	−4.61	1128	6.7×10^{-15}
$SiH_2 + H \rightarrow SiH + H_2$ (k_{2b})	10^{-3}–$10^{4}b$	4.95×10^{-10}	0.07	229	4.93×10^{-10}
	10^{-3}–$10^{4}c$	2.61×10^{-4}	−1.60	1849	
$SiH_2 + H \rightarrow SiH + H_2$ (k_{TS4})		1.05×10^{-15}	1.82	100	7.03×10^{-11}
$SiH + H_2 \rightarrow SiH_3$	k_∞	1.28×10^{-18}	2.04	1379	2.59×10^{-14}
	k_0	3.42×10^{-23}	−2.96	813	6.47×10^{-32}
	0.3	2.08×10^{-4}	−4.05	1645	8.56×10^{-17}
	1	7.38×10^{-4}	−4.06	1847	1.94×10^{-16}
$SiH + H \rightarrow {}^1SiH_2$ (k_{3a})	k_∞	5.71×10^{-12}	0.36	52	4.83×10^{-11}
	k_0	5.74×10^{-27}	−2.40	354	9.01×10^{-34}
	0.3	1.67×10^{-8}	−3.40	355	5.21×10^{-18}
	1	5.60×10^{-8}	−3.40	355	1.74×10^{-17}
	10	5.38×10^{-7}	−3.40	354	1.72×10^{-16}
	760	2.40×10^{-5}	−3.34	406	9.97×10^{-15}
$SiH + H \rightarrow {}^3Si + H_2$ (k_{3b}) via CP	10^{-3}–10^{3}	1.73×10^{-10}	−0.71	375	9.41×10^{-13}
$SiH + H \rightarrow {}^1Si + H_2$ (k_{3c})	10^{-3}–10^{3}	1.84×10^{-10}	−0.18	222.9	3.70×10^{-11}
$SiH + H \rightarrow {}^3Si + H_2$ (k_{TS5}) via TS5	10^{-3}–$10^{4}b$	1.71×10^{-9}	−0.32	299	1.26×10^{-10}
	10^{-3}–10^{4}c	2.42×10^{-7}	−0.95	915	
$SiH + H \rightarrow {}^3Si + H_2$ (k_{TS6})		1.20×10^{-15}	1.65	−4.8	3.43×10^{-11}

[a] $k(T) = AT^n \exp(-E_a/RT)$ predicted for various temperature in units of cm^3 $molecule^{-1}$ s^{-1} for k and k_∞ and cm^6 $molecule^{-2}$ $s^{-1}$for k_0 at 300–2000 K and b = 300–1000 K and c = 1000–2000 K.

to search for the MEP computed using the potential energies along the reaction coordinate (Si···H) from about 1.5 to 5.5 Å with a step size 0.1 Å at the CASPT2//CASSCF level as described earlier. The rate constants for the bimolecular reactions 1–3 and the unimolecular dissociation reactions of their corresponding excited intermediates have been derived as functions of temperature and pressure by RRKM calculations:

$$SiH_4 \rightarrow SiH_3 + H \quad (1c)$$

$$\rightarrow SiH_2 + H_2 \quad (1d)$$

$$SiH_3 \rightarrow SiH_2 + H \quad (2c)$$

$$\rightarrow SiH + H_2 \quad (2d)$$

$$SiH_2 \rightarrow SiH + H \quad (3d)$$

$${}^3SiH_2 \rightarrow {}^3Si + H_2 \quad (3e)$$

$${}^1SiH_2 \rightarrow {}^1Si + H_2 \quad (3f)$$

In the calculation of the specific rate constant, $k(E,J)$ the number of available states at the transition state is obtained at the energy E and with the total angular momentum J resolved level based on the rigid-rotor harmonic oscillator assumption for the energy levels. For the evaluation of the electronic partition function of SiH, the spin–orbit coupling energy of 142.83 cm^{-1} for $X^2\Pi$ (1/2, 3/2) is used.[42] The average energy transferred by downward collisions $\langle \Delta E_{down} \rangle$ is assumed to be 400 cm^{-1} for SiH_x and Ar collisions. Additionally, the Lennard-Jones parameters for collision rate estimates are obtained by using σ = 4.08 Å and ε = 144 cm^{-1} for SiH_4[43]; σ = 3.943 Å and ε = 118.3 cm^{-1} for SiH_3[43]; σ = 3.80 Å and ε = 92.5 cm^{-1} for SiH_2[43]; and σ = 3.75 Å and ε = 98.3 cm^{-1} for Ar.[23]

Bimolecular association of H with SiH_3 and decomposition of SiH_4

The bimolecular reaction of H and SiH_3 occurs exclusively by the association process forming the excited SiH_4 intermediate carrying as much as 90.2 kcal/mol of internal energy with 33.5 kcal/mol of excess energy above the transition state for H_2 elimination at TS1; giving the SiH_2 radical as shown by the PES

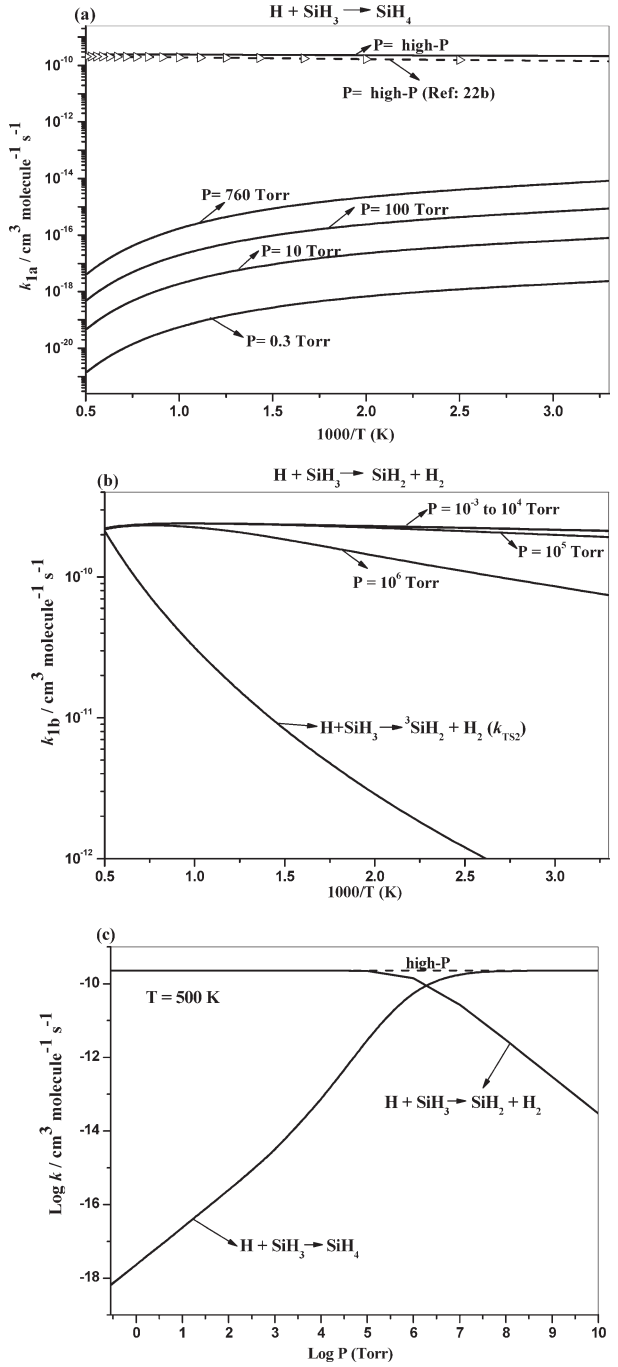

Figure 3. Arrhenius plots of rate constants for H + SiH_3 → SiH_4 a), H + SiH_3 → SiH_2 + H_2 b) at different pressures and predicted rate constants at T = 500 K as functions of pressure for H + SiH_3 producing SiH_4 and SiH_2+H_2 c).

given in Figure 1a. The predicted rate constants for both product channels at 300–2000 K temperature range and various pressures including the high- and low-pressure limits are summarized in Table 4, and the rate constants are also graphically presented in Figures 3a and 3b. The calculated pressure-dependent rate constants for competing product formation at 500 K are displayed in Figure 3c. These results clearly show that the formation of SiH_4 by collisional deactivation is strongly P-dependent and cannot compete with the H_2 elimination process at pressure less than 10^6 Torr because of its low energy barrier and the small molecular size. At 500 K, the decomposition reaction is more than 10^7 times greater than the deactivation process under practical experimental conditions. This finding indicates that under PECVD conditions (e.g., P < 1 Torr at 500 K), the SiH_3 + H reaction rapidly generates SiH_2, and the SiH_2 + H_2 reverse process is too slow to compete. Our calculated rate constant for SiH_3 + H → SiH_2 + H_2 at 300 K is 2.1 × 10^{-10} cm^3 $molecule^{-1}$ s^{-1}, which is close to the value predicted by Barbato et al.,[23] 1.2 × 10^{-10} cm^3 $molecule^{-1}$ s^{-1} from their reported expression, 1.15 × $10^{-11}T^{0.736}$ exp(134.8/T(K)) cm^3 $molecule^{-1}$ s^{-1}, using the kinetic Monte Carlo method to solve the master equation in their RRKM calculation based on PES computed at the CCSD(T)/CBS//B3lyp/aug-cc-pvtz level of theory for 300–2000 K and 10^{-3}–75 Torr pressure. Experimentally, Loh and Jasinski[44] investigated the H + SiH_3 reaction using the modeled SiH_3 densities generated

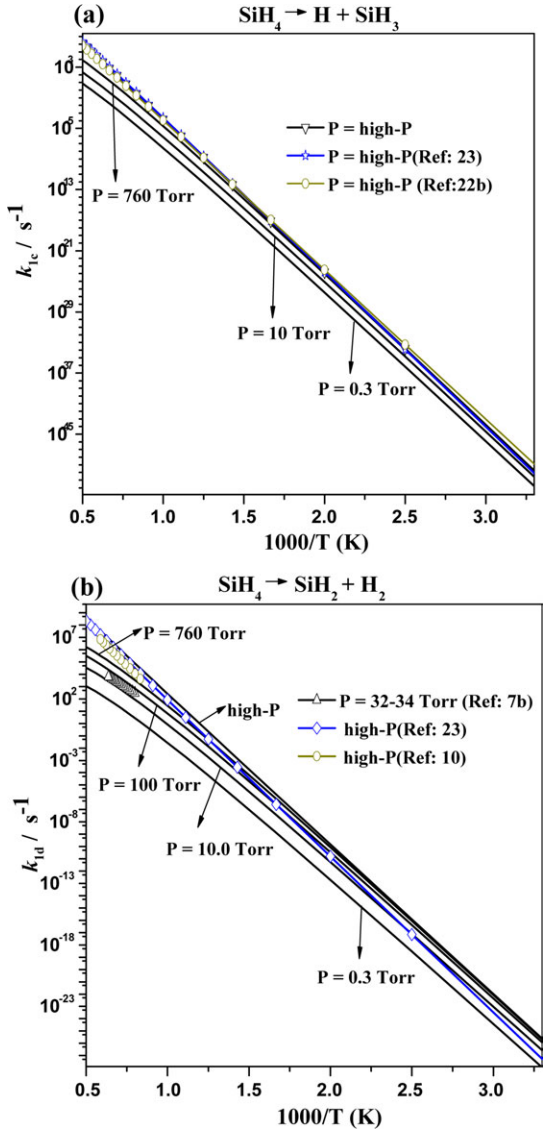

Figure 4. Arrhenius plots of rate constants for SiH_4 → H + SiH_3 a) and SiH_4 → $^1SiH_2$ + H_2 b) at different pressures. [Color figure can be viewed in the online issue, which is available at wileyonlinelibrary.com.]

Table 5. Arrhenius parameters[a] for unimolecular decomposition of SiH_x (x = 1–3) at various pressures including high-pressure limit (k_∞) and low-pressure limit (k_0).

	P (Torr)	A	n	E_a/R (K)	k_P (500 K)
$SiH_4 \rightarrow SiH_3 + H$ (k_{1c})	k_∞	1.01×10^{17}	−0.26	46,155	1.56×10^{-24}
	k_0	1.23×10^{12}	−4.86	47,295	6.68×10^{-43}
	0.3	3.74×10^{30}	−5.87	47,343	3.54×10^{-27}
	1	1.38×10^{31}	−5.88	47,394	1.08×10^{-26}
	10	1.70×10^{32}	−5.91	47,558	7.91×10^{-26}
	760	1.96×10^{33}	−5.71	48,152	9.28×10^{-25}
$SiH_4 \rightarrow {}^1SiH_2 + H_2$ (k_{1d})	k_∞	2.78×10^{12}	0.67	27,707	1.48×10^{-10}
	k_0	3.10×10^{9}	−4.6	29,348	3.36×10^{-29}
	0.3	8.98×10^{27}	−5.6	29,353	1.93×10^{-13}
	1	3.18×10^{28}	−5.6	29,368	6.32×10^{-13}
	10	4.17×10^{29}	−5.6	29,470	5.49×10^{-12}
	760	6.50×10^{30}	−5.46	30,013	8.69×10^{-11}
$SiH_3 \rightarrow {}^1SiH_2 + H$ (k_{2c})	k_∞	1.28×10^{15}	0.15	35,159	8.71×10^{-16}
	k_0	2.54×10^{4}	−3.14	35,641	8.70×10^{-36}
	0.3	1.02×10^{23}	−4.18	35,709	4.79×10^{-20}
	1	3.96×10^{23}	−4.20	35,751	1.52×10^{-19}
	10	4.47×10^{24}	−4.21	35,805	1.39×10^{-18}
	760	4.59×10^{26}	−4.26	36,079	6.24×10^{-17}
$SiH_3 \rightarrow SiH + H_2$ (k_{2d})	k_∞	5.97×10^{9}	1.23	23,120	9.52×10^{-8}
	k_0	7.97×10^{2}	−3.04	22,206	2.39×10^{-25}
	0.3	1.22×10^{22}	−4.26	23,090	3.15×10^{-10}
	1	5.91×10^{22}	−4.31	23,311	7.12×10^{-10}
	10	1.01×10^{24}	−4.38	23,773	3.04×10^{-9}
	760	8.18×10^{25}	−4.40	24,749	3.03×10^{-8}
${}^1SiH_2 \rightarrow SiH + H$ (k_{3d})	k_∞	5.19×10^{13}	0.31	38,635	9.46×10^{-20}
	k_0	1.28×10^{-2}	−1.57	38,402	3.22×10^{-40}
	0.3	3.69×10^{16}	−2.57	38,402	1.86×10^{-24}
	1	1.24×10^{17}	−2.57	38,404	6.2×10^{-24}
	10	1.28×10^{18}	−2.57	38,418	6.07×10^{-23}
	760	1.05×10^{20}	−2.59	38,757	2.23×10^{-21}
${}^3SiH_2 \rightarrow {}^3Si + H_2$ (k_{3e})	k_∞	7.17×10^{11}	0.50	22,548	4.02×10^{-7}
	k_0	1.04×10^{1}	−2.91	21,209	4.80×10^{-26}
	0.3	1.98×10^{19}	−3.84	22,270	3.44×10^{-11}
	1	6.33×10^{19}	−3.83	22,430	8.41×10^{-11}
	10	5.37×10^{20}	−3.80	22,749	4.45×10^{-10}
	760	3.20×10^{22}	−3.76	23,359	1.01×10^{-8}
${}^1SiH_2 \rightarrow {}^1Si + H_2$ (k_{3f})	k_∞	2.17×10^{13}	0.11	32,075	5.5×10^{-15}
	k_0	1.19×10^{-2}	−1.64	32,074	5.8×10^{-35}
	0.3	3.64×10^{16}	−2.65	32,080	3.37×10^{-19}
	1	1.18×10^{17}	−2.65	32,079	1.12×10^{-18}
	10	1.23×10^{18}	−2.65	32,092	1.1×10^{-17}
	760	7.50×10^{19}	−2.64	32,388	4.09×10^{-16}

[a] $k(T) = AT^n \exp(-E_a/RT)$ predicted for various temperature 300–2000 K in units of s^{-1} for k and k_∞ and cm^3 $molecule^{-1}$ $s^{-1}$for k_0.

at various time profiles following photolysis of HCl/SiH_4 at room temperature and low pressure using infrared diode laser spectroscopy; they reported an unusually small rate constant for the exothermic radical–radical reaction, $2 \pm 1 \times 10^{-11}$ cm^3 $molecule^{-1}$ s^{-1}, which an order of magnitude smaller than the computed values mentioned earlier. The rate constant for the direct H-abstraction yielding ${}^3SiH_2 + H_2$ has been calculated using TST with the Eckart tunneling corrections as shown in Figure. 3b. The rate constant is seen to be several orders of magnitude smaller than the association/decomposition process via the singlet surface due to the 4.2 kcal/mol barrier.

The result for the thermal decomposition of SiH_4 by collisional activation producing $SiH_3 + H$ and ${}^1SiH_2 + H_2$ is presented in Figure 4 for comparison with available experimental and theoretical data.[7b,10,22b,23] The decomposition reaction is dominated by the latter product channel because of its lower energy barrier. As shown in the figure and the rate constant expressions summarized in Table 5 obtained by least-squares fitting to the predicted values, both reactions have positive-pressure dependence reflecting the nature of collisional activation. At 500 K, the production of ${}^1SiH_2$ at the high-pressure limit is predicted to be 14 orders of magnitude greater than that of SiH_3, and the disparity becomes even greater at low pressures under collision-controlled conditions due to the much higher energy requirement for the formation of the latter product (see Table 5). The calculated rate constant is in good agreement with all theoretical[10,22b,23] and experimental[7b] data measured by Matsui and coworkers using a shock tube at 33 ± 1 Torr Ar pressure in the temperature range of 1250–1570 K. Their values lie within our results predicted for 10 and 100 Torr Ar pressure. The predicted rate constants for the ${}^1SiH_2 + H_2 \rightarrow SiH_4$ reaction presented at various pressures are shown in Table 4.

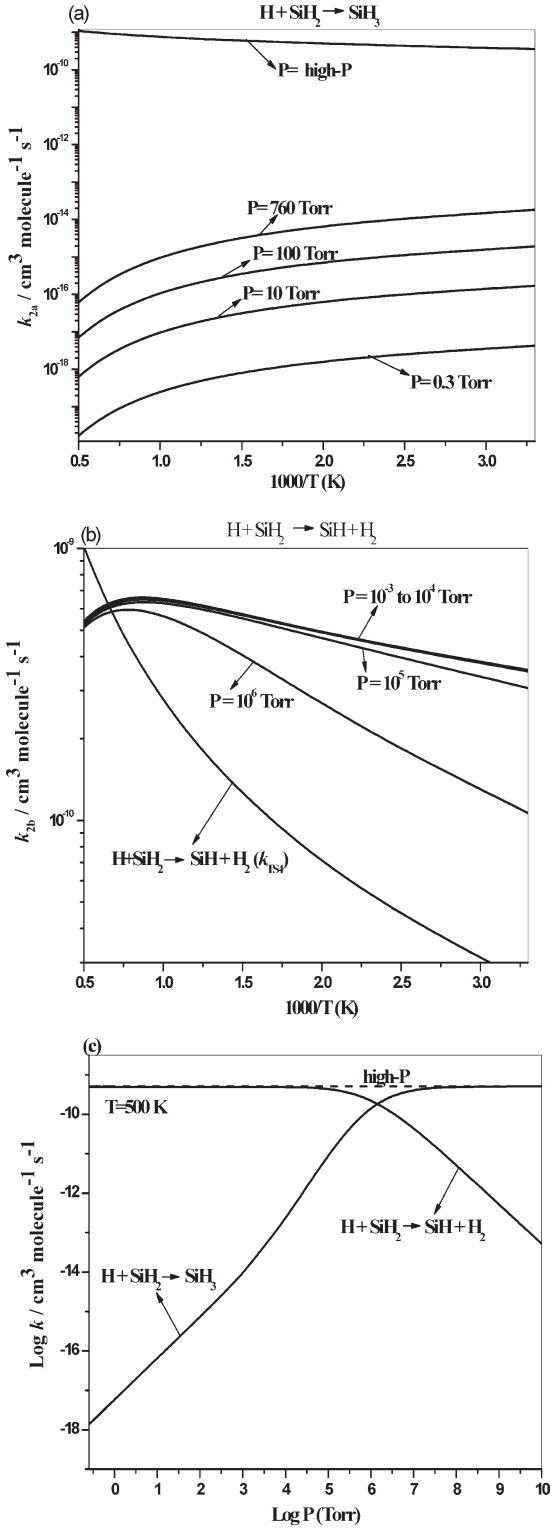

Figure 5. Arrhenius plots of rate constants for $H + SiH_2 \rightarrow SiH_3$ a), $H + SiH_2 \rightarrow SiH + H_2$ b) at different pressures and predicted rate constants at $T = 500$ K as functions of pressure for $H + SiH_2$ producing SiH_3 and $SiH+H_2$ c).

Bimolecular association of H with SiH_2 and decomposition of SiH_3

As aforementioned, the association reaction of H atom with $^1SiH_2$ producing SiH_3 with more than 68.5 kcal/mol of internal energy occurs without a well-defined transition state; the dissociation of SiH_3 can take place with 21.0 kcal/mol of excess energy above its transition state (TS3) producing H_2 and the SiH radical. The predicted values of k_{2a} forming SiH_3 at various pressures between 0.3 and 760 Torr along with its high-pressure limit in the temperature range of 300–2000 K are graphically presented in Figure 5a and are also listed in Table 4. In the table, the value for the low-pressure limit is also given for kinetic modeling. The values of k_{2a} decrease as the increasing from 300 to 2000 K. When the pressure increases from 0.3 to 760 Torr, k_{2a} increases proportionally, as clearly illustrated in Figure 5a, reflecting the need for collisional deactivation of the excited SiH_3. The predicted rate constants for the $H + SiH_2 \rightarrow SiH + H_2$ (k_{2b}) is a pressure-independent process under practical conditions as shown in Figure 5b, and their rate constant values are given by the three parameter expression covering the temperature range of 300–1000 and 1000–2000 K at 10^{-3}–10^4 Torr in Table 4. For H-abstraction reaction (k_{TS4}), the rates are smaller at low temperatures; however, as the temperature increases, they become more competitive (Fig. 5b). Accordingly,

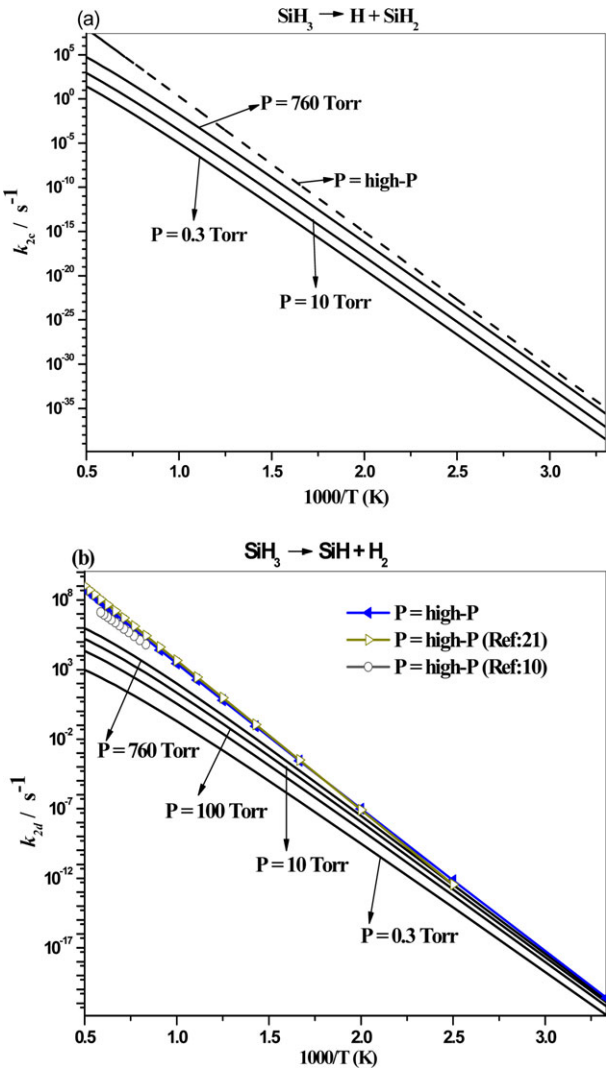

Figure 6. Arrhenius plots of rate constants for $SiH_3 \rightarrow H + SiH_2$ a) and $SiH_3 \rightarrow SiH + H_2$ b) at different pressures. [Color figure can be viewed in the online issue, which is available at wileyonlinelibrary.com.]

the rate constants for production of SiH_3 (k_{2a}) and $SiH + H_2$ (k_{2b}) at 500 K covering the wide pressure range are shown in Figure 5c. These results clearly show that the formation of SiH_3 by collisional deactivation cannot compete with the H_2 elimination process at pressures less than 10^6 Torr because of its low energy barrier and the small molecular size involved.

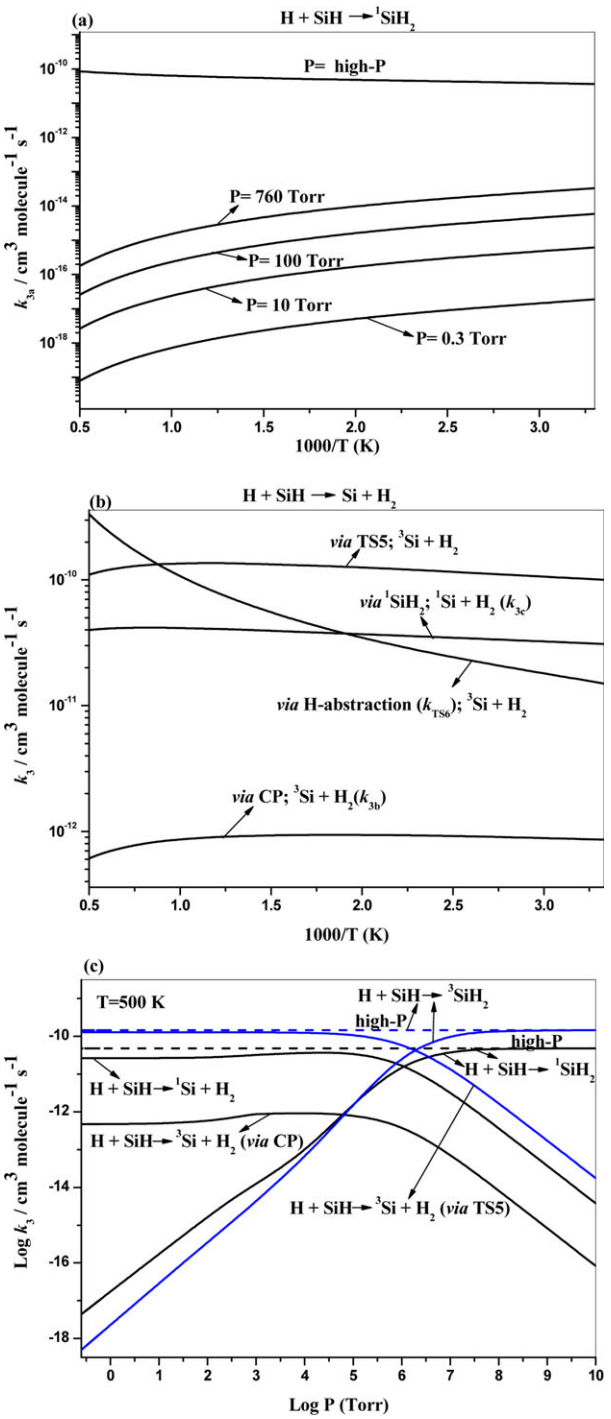

Figure 7. Arrhenius plots of rate constants for $H + SiH \rightarrow {}^1SiH_2$ a), $H + SiH \rightarrow Si + H_2$ at pressure 10^{-3}–10^3 Torr except H-abstraction b), and predicted rate constants at $T = 500$ K as functions of pressure for $H + SiH$ producing $^{1,3}SiH_2$ and $^{1,3}Si+H_2$ c). [Color figure can be viewed in the online issue, which is available at wileyonlinelibrary.com.]

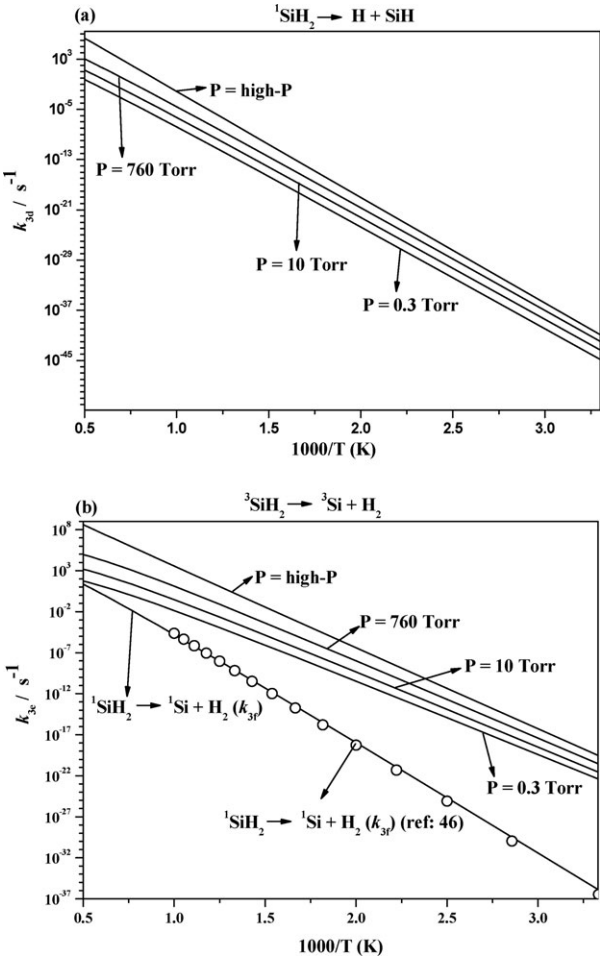

Figure 8. Arrhenius plots of rate constants for $^1SiH_2 \rightarrow H + SiH$ a) and $^3SiH_2 \rightarrow {}^3Si + H_2$ b) at different pressures. Predicted rate constant (solid line) for $^1SiH_2 \rightarrow {}^1Si + H_2$ (k_{3e}) at 1 Torr pressure in comparison with the experimental data at 1–10 Torr pressure from Ref. [46], shown in circular dots '○.'

The thermal decomposition of SiH_3 under similar conditions as given earlier for the association process produces predominantly $SiH + H_2$ due to its lower energy barrier comparing with that for $SiH_2 + H$. As shown in Figures 6a and 6b and the rate constant expressions summarized in Table 5 obtained by least-squares fitting to the predicted values, both reactions have positive-pressure dependence reflecting the nature of collisional activation. At 500 K, the production of SiH at the high-pressure limit is predicted to be eight orders of magnitude greater than that of SiH_2 production and the disparity becomes even greater at low pressures under collision-controlled conditions due entirely to the much higher energy requirement for the formation of the latter product (see Table 5). It is worth noting that, at the high-pressure limit, Walch and Dateo[21] calculated the rate constant for $SiH + H_2$ formation based on the PES computed at the CCSD(T)/a-cc-PVTZ with an extrapolation to the basis-set limit at the MP2 level; their rate constant agrees closely with our result throughout the temperature range overlapped with ours, 400–2000 K (see Fig. 6b).

Bimolecular association of H with SiH and decomposition of SiH_2

The rate constants of H + SiH reactions via singlet and triplet paths have been calculated using the molecular parameters and the energies presented in Table 2 and Figure 1c, respectively. The results for H + SiH → $^1SiH_2$ (k_{3a}), H + SiH → $^1SiH_2$* → ^3Si + H_2 (k_{3b}) via CP, H + SiH → $^1SiH_2$* → ^1Si + H_2 (k_{3c}) and the reaction via the triplet transition state TS5 are plotted in Figures 7a and 7b in the temperature range of 300–2000 K covering 0.3–760 Torr pressure. As seen from Figure 7a, the rate constant for the formation of the $^1SiH_2$ product by collisional deactivation is strongly pressure dependent and is negligibly small under practical PECVD conditions. At pressures below 10^4 Torr, formation of ^3Si + H_2 from H + SiH reaction via the chemically activated $^{1,3}SiH_2^*$ intermediates is predominant and pressure independent due to the noncompetitive quenching process as shown in Figure 7b along with the direct H-abstraction process via TS6. Comparing the contributions from the four separate paths, the formation of ^3Si + H_2 via $^3SiH_2^*$ and TS5 directly from H + SiH is dominant. At 500 K, the rate constant for this product channel is about 1–2 orders greater than those from the singlet-state path through CP and the direct abstraction via TS6 (k_{TS6}), respectively (see Fig. 7b and Table 4). The crossing probability of $^1SiH_2$ → ^3Si + H_2 spin-forbidden reaction is predicted to be 0.01–0.001 for the energy from 10 to 1000 cm^{-1} by a nonadiabatic TST calculation.[34,35] The predicted crossing probability is lower than that of Matsunaga et al.[45] who used a different method from Harvey's[35] and also used a different basis set for performing the CASSCF calculation in this energy range. The direct triplet product channel via $^3SiH_2^*$ is about three times larger than the formation of the singlet products ^1Si + H_2 via $^1SiH_2^*$. The calculated rate constant expressions for all the reaction product channels obtained by three-parameter fitting in the 300–2000 K temperature range at 0.3–760 Torr pressure are given in Table 4. The pressure-dependent rate constants for the bimolecular reactions of H + SiH forming various products calculated at 500 K are shown in Figure 7c. Apparently, at high pressure, the $^3SiH_2$ product rate constants are predicted to be around 1 order of magnitude faster than those of the singlet-state products.

The rate constant for the unimolecular decomposition of $^1SiH_2$ producing SiH + H and that for the decomposition of $^3SiH_2$ via TS5 giving ^3Si + H_2 predicted at the above-mentioned reaction conditions are shown in Figure 8. From the figure, one sees that the experimental rate constant of the $^1SiH_2$ → ^1Si + H_2 reaction reported by Johannes and Ekerdt[46] is considerably smaller comparing with that of $^3SiH_2$ → ^3Si + H_2 due to the much larger endothermicity of the former process. Predicted rate constant for $^1SiH_2$ → ^1Si + H_2 (k_{3f}) at 1 Torr pressure in comparison with the experimental[46] data at 1–10 Torr pressure are shown in Figure 8b and in good agreement.

Conclusions

The mechanism for the reactions of H atoms with SiH_x (x = 1–3) radicals and their related unimolecular decomposition processes have been investigated with *ab initio* MO calculations with the CCSD(T)/CBS extrapolation. The results show that, the reactions of H + SiH_x (x = 1–3) leading to SiH_4, SiH_3, and $^{1,3}SiH_2$ occurs with no intrinsic barriers. The excited intermediates can decompose predominantly via transition states, TS1 for SiH_4 → $^1SiH_2$ + H_2, TS3 for SiH_3 → SiH + H_2, and TS5 for $^3SiH_2$ → ^3Si + H_2, with the predicted barriers of 56.7, 47.5, and 44.3 kcal/mol, respectively. The dissociation path $^1SiH_2$ → ^1Si + H_2 was computed to be endothermic by 62.5 kcal/mol without an intrinsic barrier; however, we found a singlet–triplet surface CP locating at 16.9 kcal/mol below the ^1Si + H_2 products (or 45.6 kcal/mol from $^1SiH_2$) with the bending geometry of ∠H—Si—H = 32.9°. The H + SiH_x reactions can also take place by direct H-abstraction, the energy barriers for these processes were found to decrease according to the order, SiH_3 (4.2 kcal/mol) > SiH_2 (1.3 kcal/mol) > SiH (1.0 kcal/mol), consistent with the strengths of the corresponding Si—H bonds.

The enthalpies of the formation $\Delta_f H^\circ$ of SiH_3, SiH_2, and Si at 0 K have been predicted by using the computed enthalpies of reaction $\Delta_r H_0^\circ$, including the isodesmic reactions (SiH_x + CH_4 = SiH_4 + CH_x) at the same level. The results are in good agreement with previous experimental values. Furthermore, the rate constants for the bimolecular and unimolecular decomposition reactions for all the product channels have been calculated using the VTST method and/or the RRKM theory by solving the master equation involved over a wide range of *P,T*-conditions covering those used in a typical PECVD process.

Acknowledgments

M.C.L. also acknowledges the support from Taiwan Semiconductor Manufacturing Co. for the TSMC Distinguished Professorship and the NSC for the distinguished visiting professorship at National Chiao Tung University in Hsinchu, Taiwan. The authors are grateful to the National Center for High-performance Computing for computer time and facilities.

Keywords: *ab initio* calculation · silane chemistry · reaction mechanism · rate constant

How to cite this article: P. Raghunath, Y.-M. Lee, S.-Y. Wu, J. S. Wu, M. C. Lin, *Int. J. Quantum Chem.* **2013,** *113*, 1735–1746. DOI: 10.1002/qua.24396

Additional Supporting Information may be found in the online version of this article.

[1] (a) J. M. Jasinski, S. M. Gates, *Acc. Chem. Res.* **1991**, *24,* 9; (b) J. K. Rath, *Solar Energy Mater. Solar Cells* **2003**, *76,* 431; (c) H. Matsumura, H. Umemoto, A. Masuda, *J. Non-Cryst. Solids* **2004**, *338–340,* 19.
[2] (a) H. Matsumura, *Jpn. J. Appl. Phys.* **1991**, *30,* L1522; (b) H. S. Reehal, M. J. Thwaites, T. M. Bruton, *Phys. Stat. Sol. A* **1996**, *154,* 623.
[3] (a) H. Matsumura, *J. Appl. Phys.* **1989**, *66,* 3612; (b) I. Kobayashi, T. Ogawa, S. Hotta, *Jpn. J. Appl. Phys.* **1992**, *31*, 336.
[4] (a) P. G. Lecomber, W. E. Spear, A. Ghaith, *Electron. Lett.* **1979**, *15,* 179; (b) D. E. Carlson, C. R. Wronski, *Appl. Phys. Lett.* **1976**, *28,* 671.
[5] R. A. Street, Hydrogenated Amorphous Silicon; Cambridge University Press: New York, **1991**.

[6] M. J. Kushner, *J. Appl. Phys.* **1987**, *62,* 2803.
[7] (a) N. Itabashi, N. Nishiwaki, M. Magane, T. Goto, A. Matsuda, C. Yamada. *Jpn. J. Appl. Phys.* **1990**, *29,* 585; (b) M. Koshi, S. Kato, H. Matsui, *J. Phys. Chem.* **1991**, *95,* 1223.
[8] H. Kawasaki, H. Ohkura, T. Fukuzawa, M. Shiratani, Y. Watanabe, Y. Yamamoto, S. Suganuma, M. Hori, T. Goto, *Jpn. J. Appl. Phys.* **1997**, *36,* 4985.
[9] A. Matsuda, *Jpn. J. Appl. Phys.* **2004**, *43,* 7909.
[10] H. J. Mick, P. Roth, V. N. Smirnov, I. S. Zaslonko, *Kinet. Catal.* **1994**, *35,* 439.
[11] (a) J. P. M. Schmitt, P. Gressier, M. Krishnan, G. de Rosny, J. Perrin, *Chem. Phys.* **1984**, *84,* 281; (b) Y. Matsumi, T. Hayashi, H. Yoshikawa, S. Komiya, *J. Vac. Sci. Technol. A* **1986**, *4,* 1786.
[12] (a) J. M. Jasinski, S. M. Gates, *Acc. Chem. Res.* **1991**, *24,* 136; (b) J. M. Jasinski, S. B. Meyerson, B. A. Scott, *Ann. Rev. Phys. Chem.* **1987**, *38,* 109.
[13] N. Itabashi, K. Kato, N. Nishiwaki, T. Goto, C. Yamada, E. Hirota, *Jpn. J. Appl. Phys.* **1989**, *28,* L325.
[14] R. Viswanathan, L. M. Raff, D. L. Thompson, *J. Chem. Phys.* **1984**, *81,* 828.
[15] R. Viswanathan, D. L. Thompson, L. M. Raff, *J. Chem. Phys.* **1984**, *80,* 4230.
[16] K. F. Roenigk, K. F. Jensen, R. W. Carr, *J. Phys. Chem.* **1987**, *91,* 5732.
[17] J. G. Martin, H. E. O'Neal, M. A. Ring, *Int. J. Chem. Kinet.* **1990**, *22,* 613.
[18] H. K. Moffat, K. F. Jensen, R. W. Carr, *J. Phys. Chem.* **1991**, *95,* 145.
[19] M. D. Su, H. B. Schlegel, *J. Phys. Chem.* **1993**, *97,* 9981.
[20] (a) M. T. Swihart, R. W. Carr, *J. Phys. Chem. A.* **1998**, *102,* 1542; (b) S. W. Hu, Y. Wang, X. Y. Wang, T. W. Chu, X. Q. Liu, *J. Phys. Chem. A* **2003**, *107,* 2954; (c) S. M. Islam, J. W. Hollett, R. A. Poirier, *J. Phys. Chem. A* **2007**, *111,* 526.
[21] S. P. Walch, C. E. Dateo, *J. Phys. Chem. A* **2001**, *105,* 2015.
[22] (a) A. Dollet, S. de Persis, F. Teyssandier, *Phys. Chem. Chem. Phys.* **2004**, *6,* 1203; (b) J. Takahashi, T. Momose, T. Shida, *Bull. Chem. Soc. Jpn.* **1994**, *67,* 74.
[23] A. Barbato, C. Seghi, C. Cavalloti, *J. Chem. Phys.* **2009**, *130,* 074108.
[24] J. M. Jasinski, R. Becerra, R. Walsh, *Chem. Rev.* **1995**, *95,* 1203.
[25] M. S. Gordon, Y. Xie, Y. Yamaguchi, R. S. Grev, H. F. Schafer, III, *J. Am. Chem. Soc.* **1993**, *115,* 1503.
[26] (a) S. Y. Wu, P. Raghunath, S. J. Wu, M. C. Lin, *J. Phys. Chem. A* **2010**, *114,* 633; (b) D. H. Varma, P. Raghunath, M. C. Lin, *J. Phys. Chem. A* **2010**, *114,* 3642; (c) P. Raghunath, M. C. Lin, *J. Phys. Chem. A* **2010**, *114,* 13353.
[27] J. A. Pople, M. Head-Gordon, K. Raghavachari, *J. Chem. Phys.* **1987**, *87,* 5968.
[28] K. A. Peterson, D. E. Woon, T. H. Dunning, Jr., *J. Chem. Phys.* **1994**, *100,* 7410.
[29] D. E. Woon, Jr., T. H. Dunning, *J. Chem. Phys.* **1995**, *103,* 4572.
[30] M. J. Frisch, G. W. Trucks, H. B. Schlegel, G. E. Scuseria, M. A. Robb, J. R. Cheeseman, J. A. Montgomery, Jr., T. Vreven, K. N. Kudin, J. C. Burant, J. M. Millam, S. S. Iyengar, J. Tomasi, V. Barone, B. Mennucci, M. Cossi, G. Scalmani, N. Rega, G. A. Petersson, H. Nakatsuji, M. Hada, M. Ehara, K. Toyota, R. Fukuda, J. Hasegawa, M. Ishida, T. Nakajima, Y. Honda, O. Kitao, H. Nakai, M. Klene, X. Li, J. E. Knox, H. P. Hratchian, J. B. Cross, C. Adamo, J. Jaramillo, R. Gomperts, R. E. Stratmann, O. Yazyev, A. J. Austin, R. Cammi, C. Pomelli, J. W. Ochterski, P. Y. Ayala, K. Morokuma, G. A. Voth, P. Salvador, J. J. Dannenberg, V. G. Zakrzewski, S. Dapprich, A. D. Daniels, M. C. Strain, O. Farkas, D. K. Malick, A. D. Rabuck, K. Raghavachari, J. B. Foresman, J. V. Ortiz, Q. Cui, A. G. Baboul, S. Clifford, J. Cioslowski, B. B. Stefanov, G. Liu, A. Liashenko, P. Piskorz, I. Komaromi, R. L. Martin, D. J. Fox, T. Keith, M. A. Al-Laham, C. Y. Peng, A. Nanayakkara, M. Challacombe, P. M. W. Gill, B. Johnson, W. Chen, M. W. Wong, C. Gonzalez, J. A. Pople, Gaussian 03, Revision C.02; Gaussian, Inc.: Wallingford, CT, **2004**.
[31] S. J. Klippenstein, A. F. Wagner, R. C. Dunbar, D. M. Wardlaw, S. H. Robertson, VARIFLEX: VERSION 1.00, **1999**.
[32] (a) S. J. Klippenstein, *J. Phys. Chem.* **1994**, *98,* 11459; (b) S. J. Klippenstein, *J. Chem. Phys.* **1991**, *94,* 6469.
[33] J .A. Miller, S. J. Klippenstein, *J. Phys. Chem. A* **2000**, *104,* 2061.
[34] J. C. Lorguet, B. Leyh-Nihant, *J. Phys. Chem.* **1998**, *92,* 4778.
[35] J. N. Harvey, *Phys. Chem. Chem. Phys.* **2007**, *9,* 331.
[36] H.-J. Werner and P. J. Knowles, MOLPRO Version 2009.1 (package of ab initio programs); with contributions from J. Almlof, R. D. Amos, A. Berning et al.
[37] (a) J. Berkowitz, J. P. Greene, H. Cho, B. Ruscic, *J. Chem. Phys.* **1987**, *86,* 1235; (b) D. Husain, P. E. Norris, *J. Chem. Soc. Faraday Trans. 2* **1978**, *74,* 106.
[38] J. S. Francisco, R. Barnes, J. W. Thoman, Jr., *J. Chem. Phys.* **1988**, *88,* 2334.
[39] M. W. J. Chase, NIST-JANAF Thermochemical Tables, 4th ed.; J. Phys. Chem. Ref. Data Monogr. No. 9 (Parts I and II), **1998**, NIST, Washington DC, USA.
[40] A. M. Doncaster, R. Walsh, *Int. J. Chem. Kinet.* **1981**, *13,* 503.
[41] B. Ruscic, J. E. Boggs, A. Burcat, A. G. Csaszar, J. Demaison, R. Janoschek, J. M. L. Martin, M. L. Morton, M. J. Rossi, J. F. Stanton, P. G. Szalay, P. R. Westmoreland, F. Zabel, T. Berces, *J. Phys. Chem. Ref. Data* **2005**, *34,* 573.
[42] K. P. Huber, G. Herzberg, Molecular Spectra and Molecular Structure. Constants of Diatomic Molecules, Vol. *4; Van Nostrand Reinhold: New York,* **1979**.
[43] M. E. Coltrin, R. J. Kee, J. A. Miller, *J. Electrochem. Soc.* **1986**, *133,* 1206.
[44] S. K. Loh, J. M. Jasinski, *J. Chem. Phys.* **1991**, *95,* 4914.
[45] N. Matsunaga, S. Koseki, M. S. Gordon, *J. Chem. Phys.* **1996**, *104,* 7988.
[46] J. E. Johannes, J. G. Ekerdt, *J. Electrochem. Soc.* **1994**, *141,* 2135.

Received: 13 September 2012
Revised: 12 December 2012
Accepted: 21 December 2012
Published online on 22 February 2013